JOURNAL OF GUIDANCE, CONTROL, AND DYNAMICS
Vol. 20, No. 3, May–June 1997

Nonlinear Control of a Proof-Mass Actuator

Douglas K. Lindner,* Gregory A. Zvonar,† and Dusan Borojevic‡
Virginia Polytechnic Institute and State University, Blacksburg, Virginia 24061-0111

A proof-mass actuator is an actuator for structural control that accelerates a proof-mass in linear motion, imparting an equal and opposite force to the structure. A continuous motion of the proof-mass in one direction will eventually lead to a collision of the proof-mass with its stops, imparting shocks to the structure and possibly causing damage to the actuator. We propose nonlinear control laws for preventing collisions of the proof-mass with its stops. The linear control-loop gains are sized so that the proof-mass will not hit its stops under commanded motions. Then a nonlinear control loop is added to increase the restoring force to the proof-mass when the proof-mass is close to its stops. It is shown that the nonlinear control law increases the operating region over an actuator with only linear control loops. It is also shown that the nonlinear control law allows the mass of the actuator to be decreased while the same performance is maintained.

Nomenclature

b	= modal influence coefficient
d	= stroke length of the proof-mass
$F_{\max}$	= maximum force attainable from the electromagnetic subsystem
$f_{\max\ \text{stroke}}(\omega)$	= maximum force available from sinusoidal motion of the proof-mass
$f_{\text{pm}}(t)$	= electromagnetic force applied to the proof-mass
$f_{\text{st}}(t)$	= force applied to the structure by the proof-mass
K_n	= gain of the nonlinear control loop
K_{pa}	= gain of the actuator's position loop
K_{ps}	= gain of the structure's position loop
K_{va}	= gain of the actuator's velocity loop
K_{vs}	= gain of the structure's velocity loop
m	= mass of the proof-mass
$r_{\max}$	= value of the saturation function for command limiter
$r_{\text{pm}}(t)$	= reference input signal to the actuator control loops
$r_{\text{st}}(t)$	= reference input signal to the outer control loops
$t_s(x_0)$	= 1% settling time due to the initial condition x_0
$v_n(t) = f(y_r, \dot{y}_r)$	= nonlinear restoring force defined in Eq. (16)
$v_{\text{pm}}(t)$	= voltage input signal to the actuator
$y_{\text{pm}}(t)$, $\dot{y}_{\text{pm}}(t)$	= position and velocity of the proof-mass
$y_{\text{st}}(t)$, $\dot{y}_{\text{st}}(t)$	= position and velocity of the structure
$\zeta_{\text{ed}}(x_0)$	= equivalent damping, defined in Eq. (9)
$\zeta_{\text{PM}}(x_0)$	= performance function defined in Eq. (12)
ζ_{st}, ω_{st}	= damping and modal frequency of the structure
$\eta(t)$	= modal amplitude
ω_b	= saturation break frequency

Introduction

SEVERAL authors have proposed proof-mass actuators for vibration suppression in flexible structures.[1–16] We define a proof-mass actuator as any device that accelerates a (proof-) mass in linear motion and so generates a reaction force on the structure. This reaction force is used to suppress vibrations in the structure. These actuators are attractive because they have a favorable force-to-weight ratio. Previous work has focused on the modeling of these devices and the structure and interaction between these models, design of the vibration suppression control loops, and the experimental implementation and demonstration of enhanced damping. Most of this work is focused on the linear operation of the actuator.

Here we are concerned with the performance of a proof-mass actuator within a vibration suppression control loop for a flexible structure. The finite travel of the proof-mass, called the stroke length, imposes restrictions on the use of the actuator. The stroke length limits the amount of force available from the actuator. If the proof-mass is driven against its stops, we say the proof-mass has saturated in stroke. When an actuator saturates in stroke, shocks are imparted to the structure and damage may result. The stroke saturation defines, in part, the operating region of the actuator. Here we describe several nonlinear control laws to manage the proof-mass to prevent stroke saturation. The basic idea is that the nonlinear controller should apply an additional restoring force when the proof-mass is approaching its stops. This nonlinear control law prevents stroke saturation for a larger set of initial conditions than an actuator with only linear control laws. We then show that this region of nonsaturating initial conditions can be further enlarged by increasing the stroke length with a corresponding decrease in the mass of the proof-mass. The results here represent an alternative approach to the optimal control used by Politansky and Pilkey.[4]

Our model of the proof-mass actuator is based on a linear dc motor[3]; however, the results can be applied equally well to other configurations. The model of our actuator captures only the system level operating characteristics of the proof-mass actuators; it does not include detailed descriptions of the nonlinearities inherent in the device itself (which are realization dependent). Our purpose is to describe the operational envelope of proof-mass actuators with respect to those limitations that are common to all realizations of proof-mass actuators. These trends would be used as a guide to the selection of some of the parameters of a particular realization of the actuator.

Recently, an "error governor" controller has been proposed for systems with saturations.[17] This error governor is defined by the boundary of a set of states where the system saturates. When the system enters into a region where one of the states saturates, the error governor reduces the gain of the controller, allowing the system to return to its region of linear operation. This concept for the control of a saturating system is quite different than the nonlinear controller proposed in this paper. The controller proposed here for a proof-mass actuator recognizes that the correct action to take when the system is close to saturating is to increase the control gain and not decrease the gain as does the error governor. Also the nonlinear controller proposed here depends only on the relative position and velocity of the proof-mass and not on the rest of the states of the system; that is, it is independent of the number of modes of the system. The error governor in general depends on all of the states of the system and would require access to them. The nonlinear controller proposed in this paper offers advantages in its implementation over the error governor.

Received May 31, 1995; revision received Sept. 29, 1996; accepted for publication Jan. 9, 1997.

*Associate Professor, Bradley Department of Electrical Engineering. Member AIAA.
†Ph.D. Candidate, Bradley Department of Electrical Engineering.
‡Associate Professor, Bradley Department of Electrical Engineering.

System Model

Actuator Model

The model of the actuator and structure we use in this paper has been discussed elsewhere.[9–11,14] We summarize that development here. The actuator is composed of two primary components: the proof-mass and the base. The proof-mass has mass m (kilograms). Its range of linear motion is $2d$ (meters). We say that the actuator has a stroke of d (meters). The base contains the power electronics and other materials in a configuration that can apply a force to the proof-mass through electromagnetic coupling. The maximum force that can be applied by the electromechanical subsystem to the proof-mass is $F_{\max}$. These parameters are common to any physical realization of a proof-mass actuator.

Now, consider a proof-mass actuator attached to a flexible structure, as shown in Fig. 1, where the structure is modeled with a single flexible mode. A block diagram of the actuator and structure along with the control system components is shown in Fig. 2.

The input signal to the actuator is the voltage $v_{\mathrm{pm}}(t)$. The force $f_{\mathrm{pm}}(t)$ on the proof-mass generated by the electromechanical subsystem is assumed to be proportional to the input signal $v_{\mathrm{pm}}(t)$. (We assume that the dynamics of the electronics is on a faster time scale than the dynamics of the proof-mass.) The resulting displacement and velocity of the proof-mass are denoted by $y_{\mathrm{pm}}(t)$ and $\dot{y}_{\mathrm{pm}}(t)$, respectively, and they are identified in Fig. 2. The actuator contains two local loops to stabilize the proof-mass. (These control loops subsume the inherent stiffness and damping in the actuator.) The inner loop, labeled "actuator control loop: velocity feedback," feeds back the velocity signal with a gain of K_{va}. The outer loop is a negative unity feedback of the position of the proof-mass. This loop is labeled the "actuator control loop: position feedback." The two gains, K_{va} and K_{pa}, determine the transfer function $Y_{\mathrm{pm}}(s)/R_{\mathrm{pm}}(s)$ when the structure is constrained to be stationary [when $y_{\mathrm{st}}(t) \equiv 0$]. The design of the actuator control loops is discussed later.

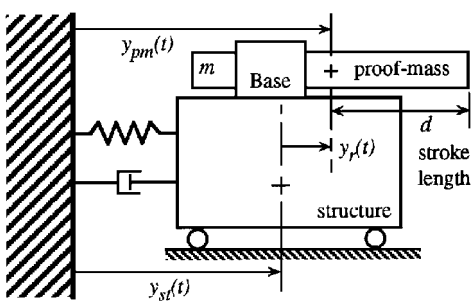

Fig. 1 Proof-mass actuator and a single-mode model.

Model of the Total System

From the full system in Fig. 2, we see that a force applied to the proof-mass, $f_{\mathrm{pm}}(t)$, results in a reaction force on the structure, $f_{\mathrm{st}}(t)$. At the location of the actuator attachment, the displacement of the structure is $y_{\mathrm{st}}(t)$. The relationship between the applied force and the resulting displacement and velocity of the structure are given by a single-mode model:

$$\ddot{\eta}(t) + 2\zeta_{\mathrm{st}}\omega_{\mathrm{st}}\dot{\eta}(t) + \omega_{\mathrm{st}}^2\eta(t) = bf_{\mathrm{st}}(t)$$
$$y_{\mathrm{st}}(t) = b\eta(t), \qquad \dot{y}_{\mathrm{st}}(t) = b\dot{\eta}(t) \tag{1}$$

In the numerical simulations that follow, the parameter values of the structure in Eq. (1) are $\omega_{\mathrm{st}} = 8.165$ rad/s, $b = 0.024$, and $\zeta_{\mathrm{st}} = 0.003$ (0.3% damping). This model assumes that there is a displacement and velocity sensor collocated with the actuator.

We consider two feedback loops to affect the vibration suppression control loops. The first loop, labeled "vibration suppression loop: position feedback" in Fig. 2, feeds back the position of the structure to the actuator with a gain of K_{ps} to the actuator reference input $r_{\mathrm{pm}}(t)$. The second loop, labeled "vibration suppression loop: velocity feedback" in Fig. 2, feeds back the velocity of the structure to the actuator with a gain of K_{vs}. The primary purpose of the vibration suppression loops is to suppress vibrations in the structure. The gains in the vibration suppression loops are chosen after the gains of the actuator control loops are fixed.

Nonlinearities

In the analysis that follows, we consider two inherent nonlinearities of the proof-mass actuator. The first nonlinearity models the saturation of the power electronics used in the actuator. We assume that this limitation can be modeled as a standard saturation nonlinearity:

$$\mathrm{sat}_T(\sigma) = \begin{cases} T, & \sigma > T \\ \sigma, & -T \le \sigma \le T \\ -T, & -T < \sigma \end{cases} \tag{2}$$

For the proof-mass actuator, the force applied to the proof-mass is modeled by Eq. (2), where $T = F_{\max}$ and $\sigma = v_{\mathrm{pm}}(t)$. This nonlinearity is identified in Fig. 2 as the "force limit."

The second nonlinearity associated with the actuator is the stroke saturation. Let the relative displacement between the proof-mass and structure be $y_r(t)$. If the relative displacement of the proof-mass is greater than stroke d, $|y_r(t)| \ge d$, then the proof-mass will run against its stops. This nonlinearity is not shown explicitly in the block diagram of the system in Fig. 2. The stroke saturation

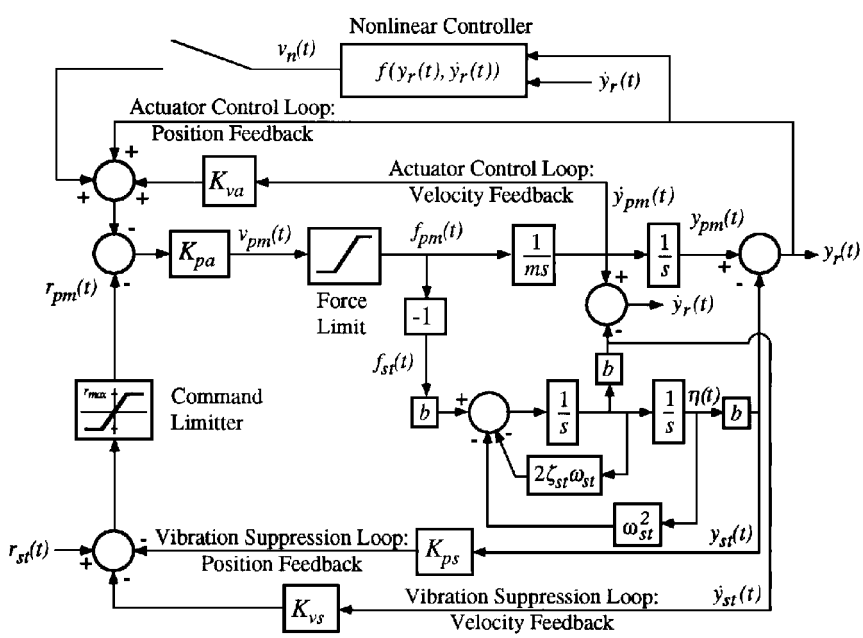

Fig. 2 Block diagram of a single-mode structure with a proof-mass actuator.

provides a boundary in the state space of the system over which the proof-mass may not cross (as discussed later). We do not consider the dynamics of the total system after the proof-mass contacts its stops.

For conciseness, we have also shown two nonlinear control elements in Fig. 2. In addition to the inherent force saturation, we will introduce a command limiter for nonlinear control of the proof-mass actuator. This command limiter is defined by

$$r_{\mathrm{pm}}(t) = \mathrm{sat}_{r_{\max}}[r_{\mathrm{st}}(t) - K_{\mathrm{vs}}\dot{y}_{\mathrm{st}}(t) - K_{\mathrm{ps}}y_{\mathrm{st}}(t)] \tag{3}$$

where the saturation function is defined in Eq. (2). This command limiter is shown in Fig. 2, and it is labeled as such. For the linear analysis in the next section we set the saturation limit of the command limiter to infinity, $r_{\max} = \infty$. Also shown in Fig. 2 is the nonlinear feedback function. This function is discussed in the next section. For the linear analysis, the switch is left open.

Linear Design of the Control Loops

Stroke/Force Saturation Curve

In this section, we review the relationship between the linear control loops of the actuator and its nonlinearities.[14] This relationship forms the basis for introducing the nonlinear control laws in the following sections. Suppose that the motion of the proof-mass is sinusoidal. Then this motion with its largest possible amplitude is

$$y_{\mathrm{pm}}(t) = d\sin(\omega t)$$

Then the maximum instantaneous force imparted to the proof-mass is

$$f_{\max\ \mathrm{stroke}} = md\omega^2 \tag{4}$$

The frequency-dependent curve Eq. (4) is plotted in Fig. 3 on a log-log scale, and it is labeled as the stroke saturation curve. The other constraint in our system is the maximum electromechanical force that can be supplied by the electromechanical subsystem $F_{\max}$. Assuming that the motion of the proof-mass is sinusoidal, this actuator nonlinearity is frequency independent. Hence, this constraint is a horizontal line shown in Fig. 3 as the force saturation curve. These two force constraints can be combined by taking the minimum value of the two curves at each frequency. The resulting curve is the stroke/force saturation curve, also shown in Fig. 3.

Define the saturation break frequency ω_b as the frequency at which the maximum force output from the motion of the proof-mass in Eq. (4) is equal to $F_{\max}$,

$$\omega_b = \sqrt{F_{\max}/md} \tag{5}$$

The saturation break frequency is identified in Fig. 3. At frequencies below the saturation break frequency, this maximum force output is determined by the product of the stroke length and the mass, md in Eq. (4). The product md is called the mass/stroke constant. Above the saturation break frequency, the maximum force output is determined by the maximum available force from the electromechanical subsystem $F_{\max}$.

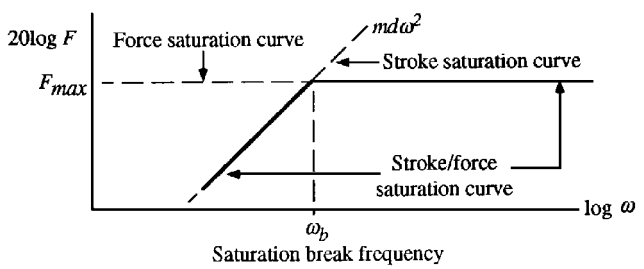

Fig. 3 Stroke/force saturation curve.

Actuator Control Loops

The stroke/force saturation curve, which contains the parameters of the actuator, is related to the actuator control gains K_{pa} and K_{va} through the frequency response of the actuator. Consider again the actuator/structure block diagram in Fig. 2 when the structure is constrained to be stationary [$y_{\mathrm{st}}(t) \equiv 0$]. The command-to-force transfer function is

$$\frac{F_{\mathrm{pm}}(s)}{R_{\mathrm{pm}}(s)} = \frac{K_{\mathrm{pa}}s^2}{s^2 + (K_{\mathrm{pa}}K_{\mathrm{va}}/m)s + (K_{\mathrm{pa}}/m)} \tag{6}$$

This is a second-order high-pass filter. The actuator bandwidth ω_a is defined as

$$\omega_a = \sqrt{K_{\mathrm{pa}}/m} \tag{7}$$

which is the corner frequency of the transfer function in Eq. (6), assuming this system has two complex poles. At low and high frequencies, the slopes of the straight line approximation of the magnitude Bode plot of Eq. (6) match the slopes of the stroke/force saturation curve. If the actuator bandwidth matches the saturation break frequency,

$$\sqrt{K_{\mathrm{pa}}/m} = \omega_a = \omega_b = \sqrt{F_{\max}/md} \tag{8}$$

then the straight line approximation of the magnitude Bode plot of Eq. (6) matches the stroke/force saturation curve. If in addition K_{va} is chosen so that the damping factor of this high-pass filter is 0.707, then the magnitude of the frequency response of Eq. (6) achieves the best match to the stroke/force saturation curve.

The correspondence between the magnitude Bode plot of the transfer function in Eq. (6) and the stroke/force saturation curve establishes a relationship between the actuator control loops; the parameters $F_{\max}$, m, and d of the actuator; and the nonlinearities of the actuator. Given the actuator with its parameters, we assume that the actuator control loops are chosen according to this criterion. This choice of the linear control loops uses the actuator to its maximum capacity.[14]

After the actuator control loops are fixed, the vibration suppression control loops are designed. For the control loops in Fig. 2, K_{vs} and K_{ps} are chosen to meet the mission requirement of the closed-loop system.[9] For concreteness, we assume in this paper that the actuator is to increase the damping of the structural mode from 0.03 to 5%.

Performance Criteria

The purpose of this paper is to evaluate the performance of the proof-mass actuator within a vibration suppression control system. (Our purpose is not to demonstrate that we can add damping to the structure.) The actuator is to be selected so that it has the authority to meet the damping specifications over the largest possible operation region, but it does not add excessive mass to the structure. For the performance evaluation, we use a performance function that was introduced previously.[10,11,14]

We focus on the transient response of the actuator to a given initial condition. Let $t_s(x_0)$ be the 1% settling time of the structure's position $y_{\mathrm{st}}(t)$, corresponding to the initial condition x_0. Define the equivalent damping $\zeta_{\mathrm{ed}}(x_0)$ as

$$\zeta_{\mathrm{ed}}(x_0) = \frac{-\ell n(0.01)}{\omega_{\mathrm{st}}t_s(x_0)} \tag{9}$$

For a linear structure, this definition of damping will coincide with the usual definition of damping for all initial conditions.

We assume that the mission requirements preclude stroke saturation of the actuator because shocks are imparted to the structure and damage may occur to the actuator itself. We quantify the stroke saturation by using the state of the system model

$$x = [y_{\mathrm{pm}} \quad \dot{y}_{\mathrm{pm}} \quad y_{\mathrm{st}} \quad \dot{y}_{\mathrm{st}}]^T \tag{10}$$

For a given set of initial conditions, we examine the closed-loop time response of the relative position of the structure and the proof-mass.

If the relative position is less than the stroke length of the actuator for $t \geq 0$, the actuator does not saturate in stroke and we say that the initial condition is in the operating region of the actuator. The operating region $\mathcal{OR}$ is the set of initial conditions, where

$$\mathcal{OR} = \left\{ x_0 = x(0) \mid \max_{t \geq 0} |y_r(t)| < d \right\} \tag{11}$$

By insisting that the actuator not saturate in stroke, we have defined hard boundaries for the operating system.

The equivalent damping captures the effect of the saturation nonlinearity in the actuator. The stroke saturation is captured by the operating region. To combine the two measures of equivalent damping and the operating region, we define the performance function ζ_{PM}:

$$\zeta_{\text{PM}} : R^4 \to R; \qquad \zeta_{\text{PM}}(x_0) = \begin{cases} \zeta_{\text{ed}}(x_0), & x_0 \in \mathcal{OR} \\ 0, & x_0 \notin \mathcal{OR} \end{cases} \tag{12}$$

Given two actuators with approximately the same equivalent damping profile, the actuator with the largest operating region is considered more desirable.

Mass Efficiency

The results in this paper are directed toward developing a sizing criterion for proof-mass actuators so that the actuator has a minimum total mass but enough authority to meet the damping specifications (mass-efficient actuators[16]). For a given total mass, the authority of the actuator is divided between the electromagnetic force applied to the proof-mass and the mass and stroke length of the proof-mass. At high frequencies, the authority of the actuator is determined by maximum force available from the electromechanical subsystem. An increase in the authority of the electromechanical subsystem will also increase the mass of the base. At low frequencies, the authority of the actuator is determined by the mass and stroke length of the proof-mass. As mass of the proof-mass is increased, the authority of the actuator is increased. These two parameters independently determine the capacity of the actuator as summarized by the stroke/force saturation curve in Fig. 3. One way to parameterize the actuator authority is to assume that the maximum force available from the electromechanical subsystem of the actuator is fixed at $F_{\max} = 30\,\text{N}$ and to vary the mass of the proof-mass. This parameterization essentially determines a lower bound on the total mass of the actuator. Although these remarks do not provide a rigorous framework for sizing the actuator, they do place the results in the following section within the context of sizing the actuator.

Performance of Linear Control of the Proof-Mass

Given the control structure in Fig. 2 and the control design strategy described in the prior section, the control loop gains will be determined by the actuator's parameters, $F_{\max}$, m, and d. The performance of the actuator within the control system will depend on the relationship between the parameters of the actuator and the structure, however. In this section, we review the performance of the actuator within the linear control loops[14] because the linear control laws form the basis for a comparison with the nonlinear controller discussed in the following sections.

To discuss the variation of the actuator performance for different parameters, we begin by fixing the structure's natural frequency at $\omega_{\text{st}} = 8.165$ rad/s as given in Eq. (1). From the analysis of the actuator's control loops, we see that the important parameter is the actuator's saturation break frequency. This constant depends on the maximum force available and the mass/stroke constant. For the simulations that follow, we fix $F_{\max}$ to 30 N and the stroke length d to 0.15 m. Then we allow the mass of the proof-mass m to vary from 1 to 10 kg. Table 1 shows the control loop gains that result from applying our design methodology to these three cases.

Case 1: $\omega_{b1} = 14.142$ rad/s $> \omega_{\text{st}}$

For this choice of parameters, the structure's natural frequency is well below the actuator's saturation break frequency. The performance function is shown in Fig. 4. Note that the performance function is defined on a four-dimensional domain. In Fig. 4 and in the figures that follow that contain a plot of the performance function, we have plotted this function on the subspace of initial conditions defined by

$$y_{\text{st}}(0) = y_{\text{pm}}(0) \qquad \text{and} \qquad \dot{y}_{\text{st}}(0) = \dot{y}_{\text{pm}}(0) \tag{13}$$

On this subspace, the proof-mass and the structure have the same displacement and velocity initially.

Table 1 Actuator and control loop parameters, cases 1–3

	m, kg	ω_b, rad/s	K_{va}	K_{pa}	K_{ps}	K_{vs}
Case 1	1	$14.142 > \omega_{\text{st}}$	0.09810	200	0	−26
Case 2	3	$8.165 = \omega_{\text{st}}$	0.17146	200	−70	0
Case 3	10	$4.472 < \omega_{\text{st}}$	0.31305	200	0	−11.5

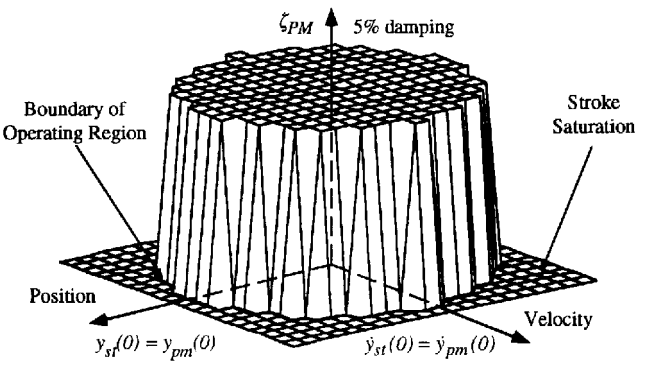

Fig. 4 Performance function for case 1.

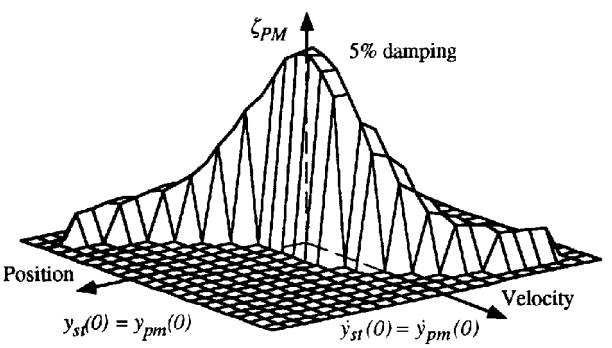

Fig. 5 Performance function for case 3.

Case 2: $\omega_{b2} = 8.165$ rad/s $= \omega_{\text{st}}$

The performance function for this choice of parameters is very much like that of Fig. 4 but with an increased operating region.[11] [The operating region is the domain of the performance function; see Eq. (11).]

Case 3: $\omega_{b3} = 4.472$ rad/s $< \omega_{\text{st}}$

The performance function for this choice of parameters is shown in Fig. 5. Note that the equivalent damping has been reduced near the extremes of the operating region. Furthermore, the operating region is skewed near the extremes. In these regions, the actuator shows pronounced nonlinear behavior. This performance function is qualitatively different than the performance function in Fig. 4. Figure 6 shows the operating region for cases 1–3.

When the actuator's saturation break frequency is equal to or greater than the structure's natural frequency, $\omega_b \geq \omega_{\text{st}}$, as in cases 1 and 2, the force available from the actuator is limited by the stroke length of the actuator (see Fig. 3). Here the stroke nonlinearity defines the operating region. The actuator exhibits linear behavior within the operating region as shown in Fig. 4, because the force saturation nonlinearity is not affecting the dynamics of the actuator in the operating region.

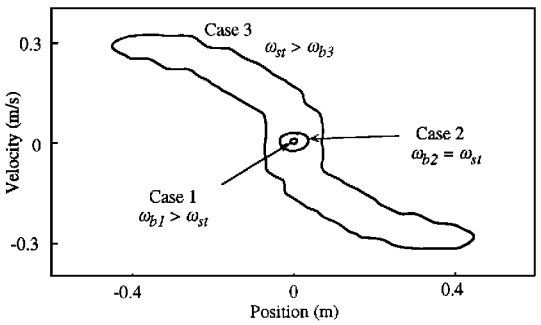

Fig. 6 Comparison of operating regions for different values of the saturation break frequency.

When the actuator's saturation break frequency is less than the structure's natural frequency, $\omega_b < \omega_{st}$, as in case 3, the operating region takes on an irregular shape. Close to the origin, the performance function matches the performance function in Fig. 4. For larger excitations, however, the force saturation nonlinearity dominates the actuator dynamics. This nonlinear response corresponds to a reduced equivalent damping at the extremes of the operating region as shown in Fig. 5 and the irregular shape of the operating region. Here the full stroke of the actuator is not being used.

These observations suggest that when the saturation break frequency matches the structure's resonant frequency, the capacity of the actuator is being used to its fullest extent.[14] At this point, we ask can nonlinear control of the proof-mass be used to further improve the performance of the actuator? We can answer this question in the affirmative.[10,11] When the actuator parameters are chosen so that the actuator saturation break frequency matches the structure's resonant frequency, the opportunity for improvement by nonlinear control is the greatest. The discussion of the nonlinear control in the next section assumes that the actuator is sized to match the structure; that is, ω_b is matched to ω_{st}.

Nonlinear Control of the Proof-Mass

In this section, we investigate the addition of nonlinear controllers to the existing proof-mass actuator for the purpose of increasing its operating region. It is assumed that the actuator is matched to the structure as described in the prior section. Consider a set of initial conditions that result in a time history that saturates in stroke, as shown in Fig. 7. Even though we do not model the stroke saturation event (notice no effect on the time history at the stroke limit), this time history contains clues on how we could increase the operating region with nonlinear control. When this saturation is taking place, the vibration suppression feedback signals are generating large control signals. This observation suggests that the reference command to the actuator should be clipped to avoid the large commands that lead to stroke saturation. The feedback signal is clipped by the command limiter, introduced in Eq. (3) and shown in Fig. 2. We set the maximum allowable value of the saturation limit at $r_{\max}$ = stroke length = d = 0.15 m because we do not wish to command excursions of the proof-mass that violate the stroke length. For this value of the command limit, the performance function is shown in Fig. 8. The command limiter serves to reduce the effective gain of the vibration suppression loop gain when the proof-mass/structure states are close to the stroke limit, because the large command signals are clipped. Hence, near the boundary of the operating region some loss of damping is expected (compare with Fig. 4), although the operating region is increased (see Fig. 11 in the next section).

A second nonlinearity for managing the actuator that suggests itself is a hard spring. When the proof-mass is close to the stops, the restoring force should grow stronger acting to prevent a collision. Adding this kind of nonlinearity does serve to increase the operating region.[10,11] Suppose, however, that the proof-mass is close to one stop but moving away from that stop. The stiff spring acts to increase the velocity of the proof-mass, causing it to overshoot into the other stop. This observation leads to the following nonlinear control law. We want to increase the stiffness only when the proof-mass is close to the stops and the proof-mass is moving toward the stop. In all other

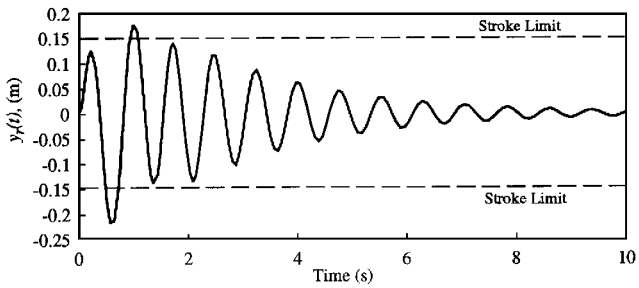

Fig. 7 Typical time response resulting in stroke saturation.

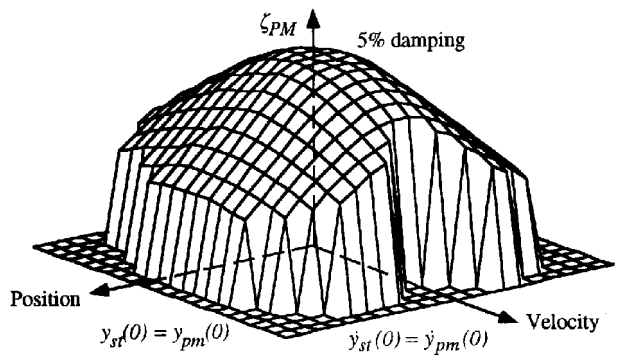

Fig. 8 Performance function with command limiter.

states, the proof-mass should be governed by the linear differential equations. To define this nonlinear control law, let

$$\operatorname{sgn}(x) = \begin{cases} 1, & x > 0 \\ 0, & x = 0 \\ -1, & x < 0 \end{cases} \tag{14}$$

Using Eq. (14), we define the nonlinear feedback function

$$v_n(t) = f[y_r(t), \dot{y}_r(t)] = \frac{K_n \dot{y}_r(t)}{\{d - y_r(t)\operatorname{sgn}[\dot{y}_r(t)]\}^2} \tag{15}$$

We call the function in Eq. (15) the position/velocity nonlinearity. When the relative position $y_r(t)$ is positive and close to the stroke length d and the relative velocity $\dot{y}_r(t)$ is positive, the denominator in Eq. (15) is small and the restoring force is large. If the relative velocity is negative, the proof-mass is moving away from the stops, the denominator is large, and a small restoring force is applied to the proof-mass.

The value of the gain K_n in Eq. (15) was chosen in the following manner. It is clear that the larger this value, the larger the operating region. This observation follows from the fact that as the value of K_n increases so does the size of the restoring force to prevent stroke saturation. Hence, the peak of the potential large excursions is reduced. At the same time, the larger the value of K_n, the more equivalent damping is sacrificed for increased operating region. Given this tradeoff, K_n was increased up to a value so that it did not affect the performance of the actuator over the original operating region. For the closed-loop system considered here, the structure's damping was 5% equivalent damping in an approximate elliptic region about ± 0.004 m by ± 0.03 m/s in Fig. 6. For the gain $K_n = 10^{-4}$, the nonlinear control system matched the damping profile over this region.

The system configuration for this nonlinear feedback loop is shown in Fig. 2 with the nonlinear switch closed. A typical time history of the relative position $y_r(t)$, when this nonlinearity is active, is shown in Fig. 9. During the initial time, the system tries to drive the proof-mass into the stops. The nonlinear controller acts to prevent the stroke saturation, but the equivalent damping is reduced. Eventually, the system decays into the linear region of operation. Here the linear controller takes over and drives the vibrations to zero. In the linear region of operation, the nonlinear controller basically contributes a small gain to the linear control loops.

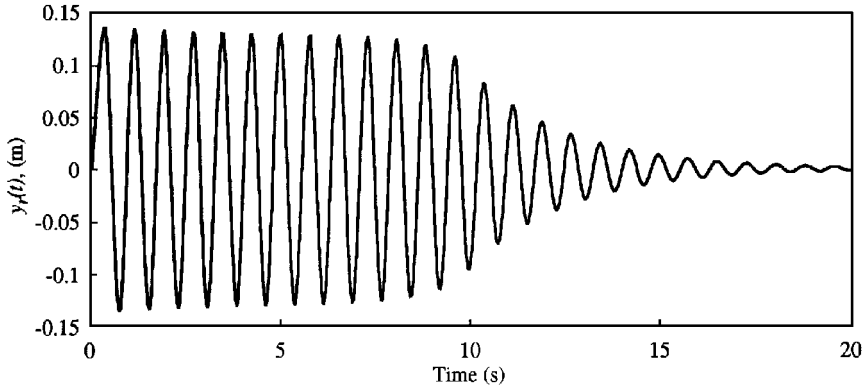

Fig. 9 Time response illustrating action of nonlinear control.

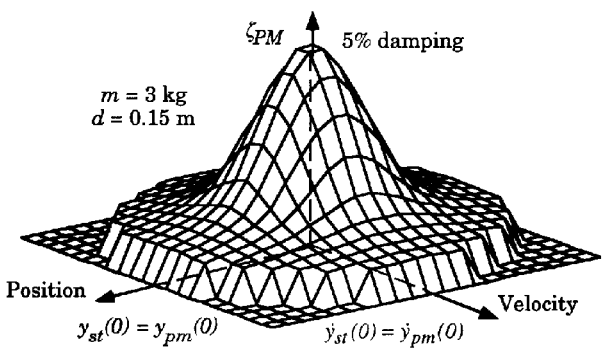

Fig. 10 Performance function with position/velocity nonlinearity.

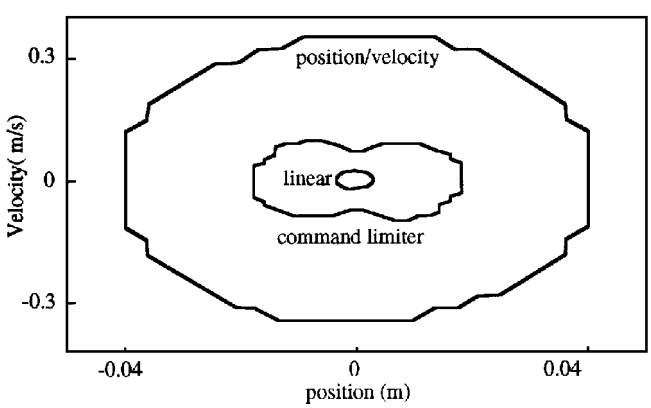

Fig. 11 Comparison of operating regions by using various nonlinear controls.

The performance function for the actuator with this nonlinear control is shown in Fig. 10.

Comparison of Controller Performance

In this section we consider nonlinear control laws to manage the proof-mass to prevent stroke saturation. We added the command limiter and the position/velocity nonlinearity to the linear control loops. The operating region for each of these systems is shown in Fig. 11.

All of the performance functions for these three systems have approximately the same value of the effective damping on the operating region of the linear design. From Fig. 11, we see that the command limiter and the position/velocity nonlinearity serve to extend the operating region of the proof-mass actuator without decreasing the performance over the operating region of the linear design. A comparison of the performance function in Figs. 4, 8, and 10 shows that the increase in the operating region is accompanied by a decrease in the equivalent damping outside the region of linear operation as would be expected.

In the preceding section, we saw that the operating region of the proof-mass actuator could be increased by increasing the mass of the proof-mass. The operating regions of the actuator with a 3-kg proof-mass with nonlinear control (shown in Fig. 11) is compared to the operating region of the actuator with a 10-kg proof-mass with linear control in Fig. 12. The actuator with the nonlinear control achieves a larger operating region with a smaller proof-mass. Thus, the total mass of the actuator can be decreased without any loss of authority with the use of nonlinear control of the proof-mass.

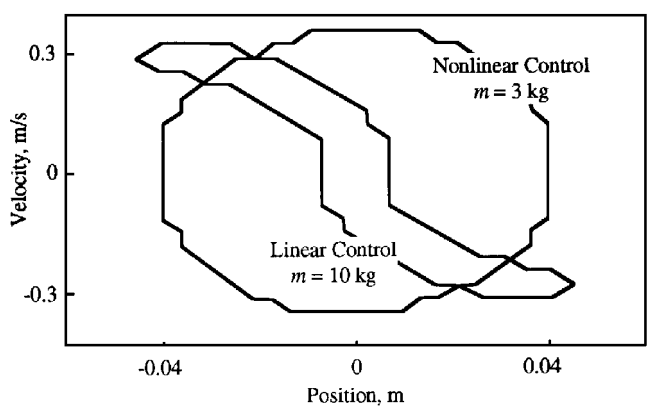

Fig. 12 Comparison of large-mass linear control and small-mass nonlinear control.

Effects of Mass and Stroke Length on Actuator Performance

In the prior section, we examined an actuator with a mass m of 3 kg, a stroke d of 0.15 m, and a force limit $F_{\max}$ of 30 N. The mass and stroke were chosen so that the saturation break frequency was matched to the structure's modal frequency. (The force limit is assumed to be fixed.) But there are many choices of the mass and stroke parameters that match these two frequencies. In particular, the saturation break frequency does not change when the mass/stroke product (md) is constant. We now examine the performance of the actuator for three different values for the mass and the stroke of the proof-mass so that the mass/stroke product remains constant. The parameter values and gains of these designs are shown in Table 2.

When only linear control loops are used, all sets of parameters have the same performance function as in case 2 (Ref. 11). Evidently, trading off the mass against the stroke has very little effect on the performance of proof-mass actuators with only linear control loops.

The performance of the actuator was determined for cases 4–6 with the limiter and position/velocity nonlinearity in actuator control loop. Qualitatively, the performance function for each actuator control system is similar to the performance function for the position/velocity nonlinearity for the mass/stroke product in Fig. 10, except that the operating region varies for different values of the stroke length.[11] A comparison between the operating regions of all three sets of actuator parameters in Table 2 is shown in Fig. 13.

Figure 13 shows a clear trend of increasing operating regions for decreasing mass of the proof-mass. We can draw two conclusions from this observation. First, the operating region can be increased by reducing the mass of the proof-mass while maintaining

Table 2 System parameters for mass/stroke constant md = 0.45 kg-m

	m, kg	d, m	K_{pa}	K_{ps}	K_n
Case 4	1	0.45	66.67	−211.2	10^{-3}
Case 5	3	0.15	200	−70	10^{-4}
Case 6	10	0.045	666.67	−20.22	10^{-5}

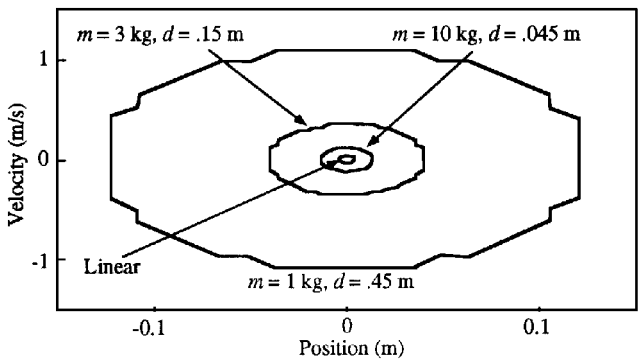

Fig. 13 Comparison of operating region with mass/stroke product constant.

the mass/stroke product constant. Because the stroke/force product is constant, the actuator retains its authority in the linear region while expanding its operating region.

Second, in Fig. 13 the linear operating region is the same for all sets of actuator parameters. So Fig. 13 shows the incremental increase in the operating region from linear control to nonlinear control. The incremental increase in the operating region for the 10-kg proof-mass is less than the corresponding increase for the 1-kg proof-mass. That is, if the mass of the proof-mass is increased, then the benefits of nonlinear control of the proof-mass are decreased. Evidently proof-mass actuators with large mass and short stroke do not benefit proportionally over a proof-mass with low mass but large stroke from the addition of nonlinear control laws to manage the proof-mass.

Stability

The presence of the nonlinear control loop introduces nonlinear dynamics into this system. The origin of this system is an equilibrium point. This equilibrium point is asymptotically stable because the system is essentially linear in this operating region. Note that the saturation functions of the form in Eq. (2) are linearized to a gain of one and the position/velocity nonlinearity Eq. (15) has a linear gain of zero. We therefore see that the linearized system is asymptotically stable, which implies that the origin of the nonlinear system is also asymptotically stable.

It is still possible that the nonlinear system could exhibit limit cycles. Therefore, it is prudent to perform nonlinear analysis on the existing system to look for such behavior.[11,13] Analysis indicates that the nonlinear control laws presented here do not cause any negative effects.

Conclusions

In this paper, we have proposed a nonlinear controller for a proof-mass actuator to manage the proof-mass. We have shown that this nonlinear controller will increase the operating region of the actuator without sacrificing the damping enhancement of the linear control loops. In addition it was found that when nonlinear control was employed, the operating region could be further increased by decreasing the mass of the proof-mass and increasing the stroke limit so that their product remained constant. These results show that the nonlinear control can be used to improve the mass efficiency over a proof-mass actuator with only linear control.

References

[1]Zimmerman, D. C., Horner, G. C., and Inman, D. J., "Microprocessor Controlled Force Actuator," *Journal of Guidance, Control, and Dynamics*, Vol. 11, No. 3, 1988, pp. 230–236.

[2]Hallauer, W., and Lamberson, S., "Experimental Active Vibration Damping of a Plane Truss Using Hybrid Actuation," *Proceedings of the AIAA/ASME/ASCE/AHS/ASC 30th Structures, Structural Dynamics, and Materials Conference* (Mobile, AL), AIAA, Washington, DC, 1989, pp. 80–89.

[3]Ham, F., Greeley, S., and Henniges, B., "Active Vibration Suppression for the Mast Flight System," *IEEE Control Systems Magazine*, Vol. 9, No. 1, 1989, pp. 85–90.

[4]Politansky, H., and Pilkey, W. D., "Suboptimal Feedback Vibration Control of a Beam with a Proof-Mass Actuator," *Journal of Guidance, Control, and Dynamics*, Vol. 12, No. 5, 1989, pp. 691–697.

[5]Sulla, J., Juang, J., and Horta, L., "Analysis and Application of a Velocity Command Motor as a Reactor Mass Actuator," *Proceedings of the AIAA Dynamics Specialist Conference* (Long Beach, CA), AIAA, Washington, DC, 1990, pp. 360–370 (AIAA Paper 90-1227).

[6]Haviland, J. K., Lim, T. M., Pilkey, W. D., and Politansky, H., "Control of Linear Dampers for Large Space Structures," *Journal of Guidance, Control, and Dynamics*, Vol. 13, No. 2, 1990, pp. 234–240.

[7]Inman, D. J., "Control/Structure Interaction: Effects of Actuator Dynamics," *Mechanics and Control of Large Flexible Structures*, edited by J. L. Junkins, Vol. 129, Progress in Astronautics and Aeronautics, AIAA, Washington, DC, 1990, pp. 507–533.

[8]Zimmerman, D. C., and Inman, D. J., "On the Nature of the Interaction Between Structures and Proof-Mass Actuators," *Journal of Guidance, Control, and Dynamics*, Vol. 13, No. 1, 1990, pp. 82–88.

[9]Lindner, D. K., Celano, T., and Ide, E., "Vibration Suppression Using a Proofmass Actuator Operating in Force/Stroke Saturation," *Journal of Vibration and Acoustics*, Vol. 113, No. 4, 1991, pp. 423–433.

[10]Zvonar, G. A., Lindner, D. K., and Borojevic, D., "Nonlinear Control of a Proof-Mass Actuator to Prevent Stroke Saturation," *Proceedings of the Eighth Symposium on Dynamics and Control of Large Structures*, Virginia Polytechnic Inst. and State Univ., Blacksburg, VA, 1991, pp. 37–48.

[11]Zvonar, G. A., "Performance Improvement of a Proof-Mass Actuator Using Nonlinear Control," M.S. Thesis, Bradley Dept. of Electrical Engineering, Virginia Polytechnic Inst. and State Univ., Blacksburg, VA, Dec. 1991.

[12]Hagood, N. W., and Crawley, E. F., "Experimental Investigation of Passive Enhancement of Damping for Space Structures," *Journal of Guidance, Control, and Dynamics*, Vol. 14, No. 6, 1991, pp. 1100–1109.

[13]Lindner, D. K., Zvonar, G. A., and Borojevic, D., "Limit Cycle Analysis of a Nonlinear Controller for a Proof-Mass Actuator," *Proceedings of the AIAA Dynamics Specialists Conference* (Dallas, TX), AIAA, Washington, DC, 1992, pp. 585–594.

[14]Lindner, D. K., Zvonar, G. A., and Borojevic, D., "Performance and Control of a Proof-Mass Actuator Accounting for Stroke Saturation," *Journal of Guidance, Control, and Dynamics*, Vol. 17, No. 5, 1994, pp. 1103–1108.

[15]Dosch, J., Lesieutre, G., Koopmann, G., and Davis, C., "Inertial Piezoceramic Actuators for Smart Structures," *Proceedings of the 1995 North American Conference on Smart Structures and Materials*, Vol. 2447 (San Diego, CA), Society of Photo-Optical Instrumentation Engineers, Bellingham, WA, 1995, pp. 14–25.

[16]Garcia, E., Webb, S., and Duke, J., "Passive and Active Control of a Complex Flexible Structure Using Reaction Mass Actuators," *Journal of Vibration and Acoustics*, Vol. 117, No. 1, 1995, pp. 116–122.

[17]Gilbert, E. G., and Tan, K. T., "Linear Systems with State and Control Constraints: The Theory and Application of Maximal Output Admissible Sets," *IEEE Transactions on Automatic Control*, Vol. 36, No. 9, 1991, pp. 1008–1020.